PARAMETERS AFFECTING THE SPATIAL RESOLUTION OF A SUPERCONDUCTING SOLENOID

by

PHILIP R. KESTEN

Submitted in Partial Fulfillment
of the Requirements for the
Degree of Bachelor of Science at
the
MASSACHUSETTS INSTITUTE OF TECHNOLOGY

June, 1978

Signature of Author . . . . . .
Department of Physics, May 19, 1978

Certified by. . . . . .
Thesis Supervisor

Accepted by . . . . . .
Chairperson, Departmental Committee on Theses

PARAMETERS AFFECTING THE SPATIAL RESOLUTION OF A SUPERCONDUCTING SOLENOID

by

PHILIP R. KESTEN

Submitted to the Department of Physics

on May 19, 1978, in partial fulfillment of the requirements

for the Degree of Bachelor of Science

ABSTRACT

Various parameters can affect the focusing of a beam of charged particles by a superconducting solenoid. This paper examines some of these parameters with regard to the spatial resolution of such a lens. A brief outline of the theory of focusing solenoids is included to provide the reader with needed background information.

Thesis Supervisor: Lee Grodzins
Professor of Physics

ACKNOWLEDGMENTS

I would like to extend my thanks to Dr. Harald Enge and to Dr. Stanley Kowalski for many helpful conversations, and especially to Professor Lee Grodzins, without whose aid and patience I would never have completed this work.

I must also thank some very special people for their encouragement and moral support, not only throughout this project, but also throughout all my years at MIT -- thanks Mom, Dad, Dan, Sue, Susie, and Peggy. And Doug and Paul -- there are no words to fully express my gratitude for your help in those last, darkest hours. If I owe this all to anyone, it is to the two of you.

TABLE OF CONTENTS

LIST OF FIGURES

INTRODUCTION

In an ideal situation, after a magnetic lens has been designed and built, it will perform according to the desired specifications. These specifications are directly related to the various parameters, associated with both the geometry of the experiment and the lens, which affect the spatial resolution of the solenoid. Certain parameters will be fixed, or have very little freedom, so that the goal of such an investigation is to find the dependence of these parameters on the other more-or-less free ones, as well as to work out the parameters for optimum focusing.

In the set-up with which I have been involved, the image length, for example, is considered to be fixed; that is, it may be varied only slightly. The position of the beam axis relative to the lens axis, on the other hand, is not fixed by the geometry. Thus it is imperative to know the dependence of the image length on the beam positioning. Naturally, one will also be concerned with the quality of the focus as a function of this parameter.

This paper, then, deals with the various free and fixed parameters associated with a specific superconducting focusing solenoid, which is to be incorporated in the scanning proton microprobe being constructed at Lincoln Laboratories under the supervision of Professor Lee Grodzins (cf. Thesis by Raymond Boisseau, 1978). Also, a brief outline of the theory of focusing solenoids is included to provide the reader with essential background information.

THEORY

Let us determine the motion of a charged particle directed through a finite solenoid lens, sometimes referred to as a "short coil". The particle has a given mass m, a charge q, and a velocity with three components, v_r, v_θ, v_z, where the z axis corresponds to the primary axis of the solenoid. The magnetic field has a radial component B_r (r, z) and an axial component B_z (r, z), but no tangential component, since the solenoid is symmetric in θ. Thus, from the Lorentz force equation,

$$\vec{F} = q\,(\vec{E} + \vec{v} \times \vec{B})$$

we find the following components for the force on the particle:

$$F_r = qv_\theta B_z \qquad (1a)$$

$$F_\theta = qv_z B_r - qv_r B_z \qquad (1b)$$

$$F_z = -qv_\theta B_r \qquad (1c)$$

These alone are sufficient to give us a general idea of the particle's motion, if we realize that while the magnetic field is fairly uniform and axial in a region inside the solenoid (region c in Figure 1), it is predominantly radial in the regions in front of and behind the lens (regions b and d). We see, then, that the particle, after having followed a straight path through region a (where the field is negligible), experiences a force in the θ direction as it passes through region b, causing it to assume a helical path. In region c,

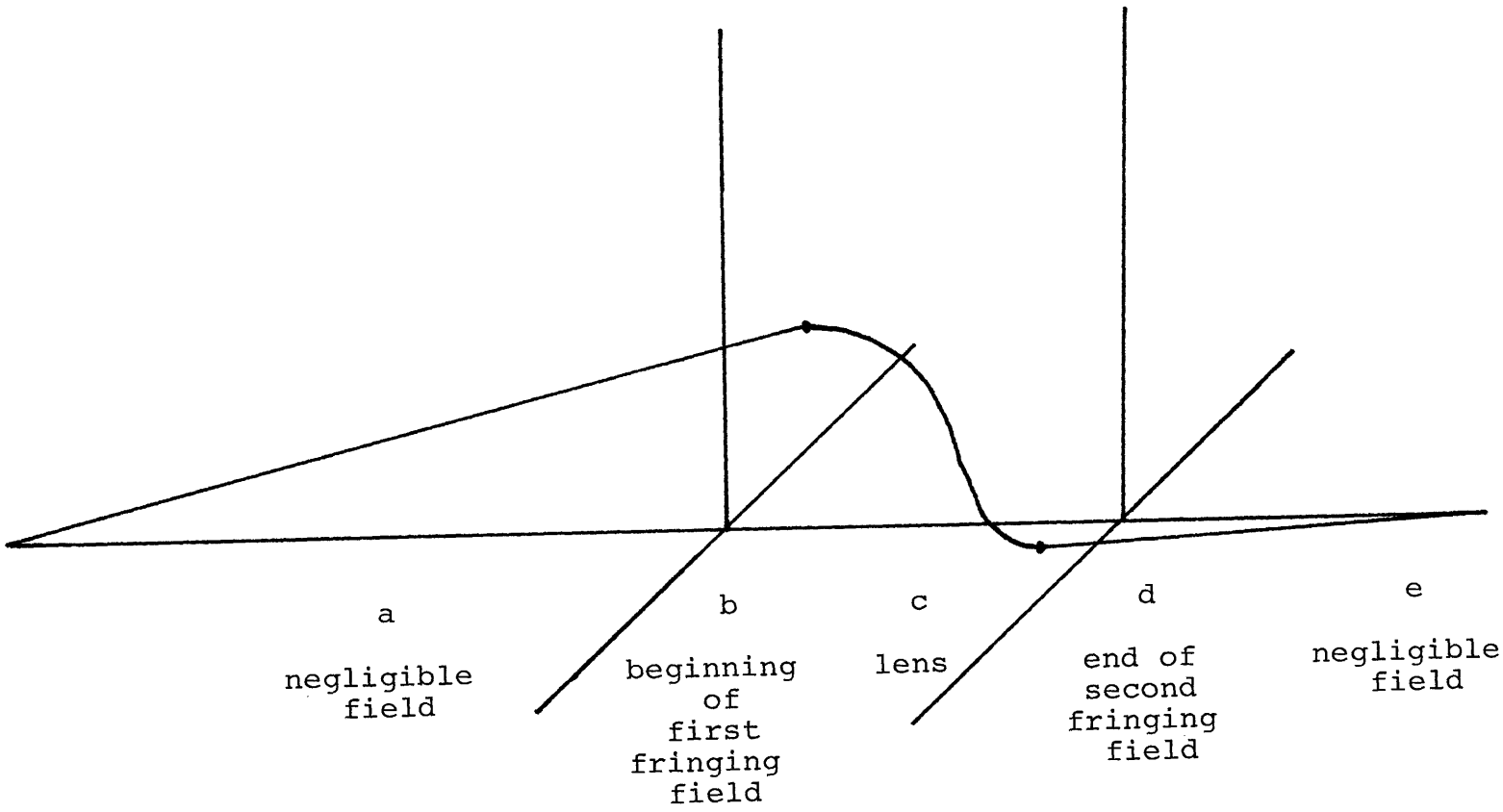

FIGURE 1

"GENERAL" PATH OF PROTON THROUGH LENS

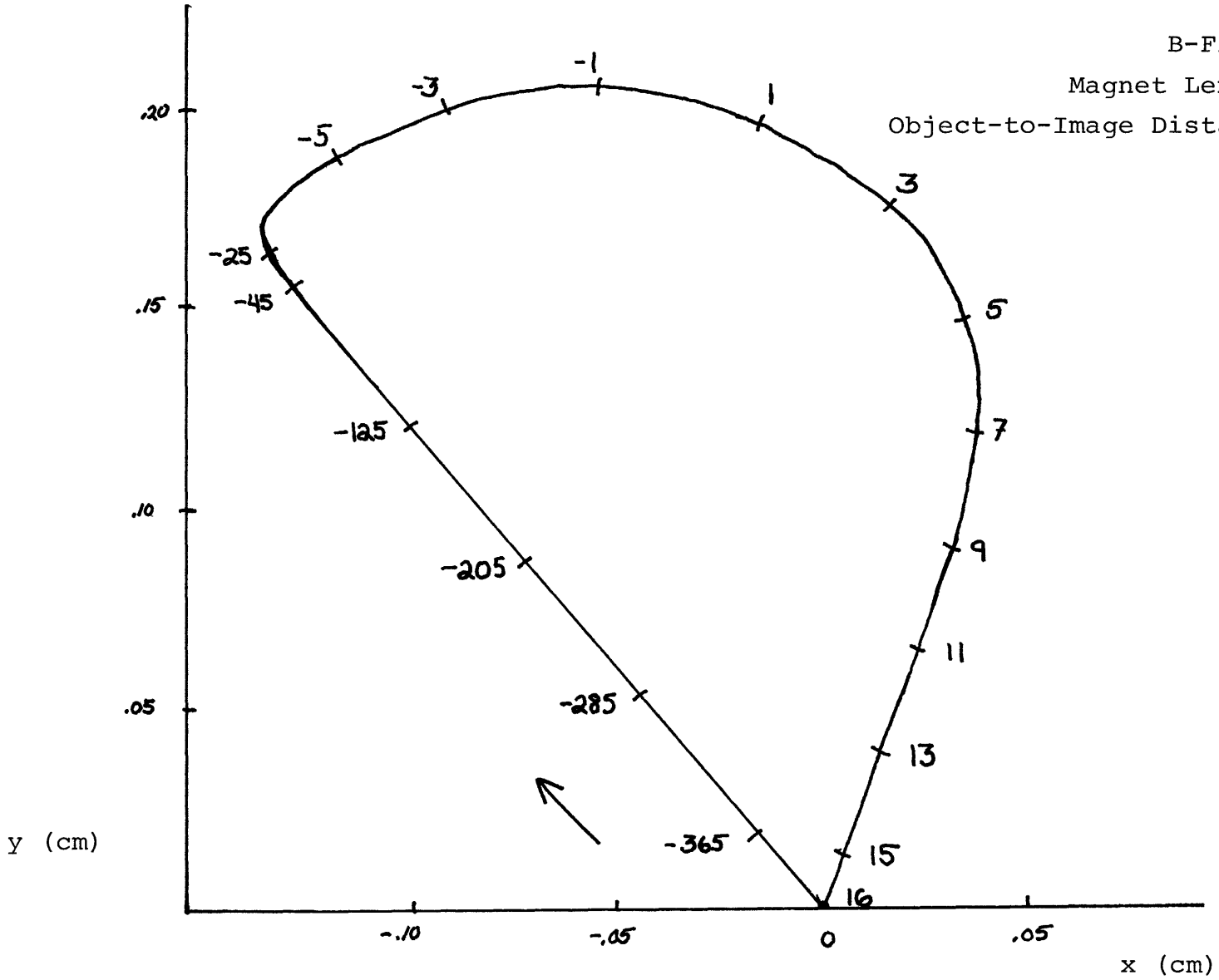

FIGURE 2

END-ON VIEW

the particle feels a radial force, due to the axial B field and tangential velocity caused by the spiraling effect of the θ force. Thus, it begins to be pulled towards the axis as it continues to spiral. In region d, B_r is again dominant, but as the particle has changed it orientation with respect to the lens, B_r is no longer in the same direction. The resulting θ force, then, tends to negate the spiral motion, so that the particle continues to travel back towards the axis. An end-on view of the particle reveals this combination spiral-focusing motion (see Figure 2) and one can also note that as the particle passes into the second fringing field, its v_θ does in fact decrease. Finally, since in region b the field is more radial with increasing distance from the axis, the tangential velocity is radially dependent; thus, the farther from the axis a particle enters the field, the larger the radial force it will feel, and the more it will be bent.

We can, however, be more precise in discussing the particle's path, by deriving its equations of motion. Defining the vector potential $\vec{A}$, such that $\vec{B}$ - curl $\vec{A}$, we get

$$B_r = - \frac{\partial}{\partial z} A_\theta \qquad (3a)$$

$$B_z = \frac{1}{r} \frac{\partial}{\partial r} (rA_\theta) \qquad (3b)$$

Thus, equation (1c) transforms to

$$F_z \ (=m\ddot{z}) = qr \dot{\theta} \frac{\partial}{\partial z} \ (A_\theta).$$

A clever method for finding θ involves realizing that

$$\vec{r} \times \vec{F} = \frac{\partial}{\partial t} (\vec{r} \times \vec{p}) \rightarrow \vec{r}F_\theta = \frac{\partial}{\partial t} (m\vec{r}^2\dot{\theta})$$

From equation (1b), with (3a,b)

$$\vec{r}F_\theta = \vec{r} \left(-q\dot{z} \frac{\partial A_\theta}{\partial z} - q\dot{r} \frac{1}{\vec{r}} \frac{\partial}{\partial r} (\vec{r}A_\theta)\right)$$

Because of symmetry, there is only a θ component of $\vec{A}$, thus $\vec{A} \equiv \vec{A}_\theta$. Then

$$\vec{r}F_\theta = -q\vec{r} \frac{\partial z}{\partial t} \frac{\partial \vec{A}}{\partial z} - q \frac{\partial r}{\partial t} \frac{\partial}{\partial r} (\vec{r}\vec{A})$$

$$= -q \frac{\partial}{\partial t} (\vec{r}\vec{A})$$

so that

$$\frac{\partial}{\partial t} (m\vec{r}^2\dot{\theta}) = -q \frac{\partial}{\partial t} (\vec{r}\vec{A})$$

Or, finally

$$\dot{\theta} = \frac{-q\vec{A}}{m\vec{r}} \qquad (4)$$

which is true for all particles returning to the axis. (See Appendix 1.) Thus, combining (2) and (4), we find the equation for the longitudinal or axial accelleration:

$$\ddot{z} = q \frac{\vec{r}}{m} \left(\frac{q\vec{A}}{m\vec{r}}\right) \frac{\partial \vec{A}}{\partial z} = \left(\frac{q}{m}\right)^2 \vec{A} \frac{\partial A}{\partial z} \qquad (5)$$

Also, since

$$m\ddot{r} = F_r + m\vec{r}\dot{\theta}^2$$

we find, using (3) and (4), that

$$m\ddot{r} = \frac{-q^2}{m} \frac{\vec{A}}{\vec{r}} \frac{\partial}{\partial r} (\vec{r}\vec{A}) + m\vec{r} \left(\frac{q}{m}\right)^2 \left(\frac{\vec{A}}{\vec{r}}\right)^2$$

By expanding the first term and regrouping, we get

$$\ddot{r} = \left(\frac{q}{m}\right)^2 \left(-\vec{A} \frac{\partial \vec{A}}{\partial r}\right) \qquad (6)$$

Equations (5) and (6) can be combined to get the actual trajectory equation, relating $\vec{r}$ and $\vec{z}$:

$$\ddot{r} = - \frac{\partial r}{\partial z} \left(\frac{q}{m}\right)^2 \vec{A} \frac{\partial \vec{A}}{\partial z} + \dot{z}^2 \frac{\partial^2 r}{\partial z^2} \qquad (7)$$

This equality, though a most important one in the consideration of solenoid lenses, is not directly applicable to the problem I have been examining. It can, however, be used as a stepping stone to a much more useful relationship, by making two first-order approximations:

First, from the definition of $\vec{A}$, over an interval with $\vec{B}$ constant,

$$\vec{B} = \oint \frac{\vec{A} ds}{\text{area}} \rightarrow \vec{B} \cdot \pi r^2 = \vec{A} 2\pi r$$
$$\rightarrow \vec{A} = \frac{\vec{B} r}{2} \qquad (8)$$

Second, since the object-to-image length is large compared to any possible $\vec{r}$, we can allow

$$\vec{r} = r_o \ .$$

Thus, we can transform (7) to

$$\dot{z}^2 \frac{\partial^2 \vec{r}}{\partial z^2} - \left(\frac{q}{m}\right)^2 \left(\frac{r_o^2 \vec{B}}{4}\right) \frac{\partial \vec{B}}{\partial z} \frac{\partial \vec{r}}{\partial z} + \left(\frac{q}{m}\right)^2 \left(\frac{B^2 r_o}{4}\right) = 0$$

or, to complete the first order approximation

$$\dot{z}^2 \frac{\partial^2 r}{\partial z^2} + r_o \left(\frac{q}{m}\right)^2 \left(\frac{B}{2}\right)^2 = 0$$

When this is integrated over the bounds of the lens, we get

$$\left.\frac{\partial \vec{r}}{\partial z}\right|_{\text{second edge}} \approx -r_o \int_{-\infty}^{\infty} B_z^{\,2}\, dz$$

and, since by the geometry,

$$-\left.\frac{\partial r}{\partial z}\right|_{\text{second edge}} = \frac{r_o}{f}$$

where f is the focal length, we have the important relation

$$\frac{1}{f} \approx \int_{-\infty}^{\infty} B_z^{\,2}\, dz$$

It should also be noted that (8), combined with (4), yields

$$\dot{\theta} = \frac{-q\vec{B}}{2m}$$

thus

$$\Theta \approx -\int_{-\infty}^{\infty} B_z\, dz$$

SOFTWARE AND HARDWARE

All the computer-generated data for this project was obtained using the RAYTRACE program written by S. Kowalski. RAYTRACE itself is a master program which allows one to call various subroutines in an order designed to model a particle's path through a particular arrangement of magnetic lenses. The main routine reads in the so-called problem definition cards, which contain such vital information as the particle's energy and momentum. Using this data, it "sets up" for the execution of the desired subroutines.

Most of my work called for the subroutine SOLND which calculates the paths of given particles or rays through a current-sheet solenoid by numerical integration of the equations of motion. Among the arguments of this routine are the length, diameter and maximum B-field of the solenoid. SOLND calls another subroutine, BSOL, which calculates the components of the B-field in the fringing region of the lens, by means of elliptic integrals. One other main subroutine I used is LENS, which, given the x_o, y_o, θ and ϕ of each ray (see Figure 4), translates the rays from the object point to some other position, say the center of the magnet.

After the paths of the rays have been determined, a two-dimensional coordinate system is set up, the origin of which corresponds to the point on the z-axis (ray 1) where the projection of ray 2 crosses. The coordinates of each ray as they cross the plane of this system (given as x_o and y_o),

along with their instantaneous slopes at that point, constitute a major portion of the output from RAYTRACE.

The RAYTRACE program as I was given it is set up to run with electrons. Thus, to simulate a proton fired from Lincoln Laboratory's Van de Graaff, E ≈ 2.5 MeV, the following approximation is made:

$$E = \frac{p^2}{2m_p c^2} \qquad \text{for these protons}$$

$$M_p c^2 \approx 1000$$

$$\rightarrow \quad p \approx \sqrt{5000} \approx 70 \quad \frac{\text{MeV}}{\text{C}}$$

The magnet whose properties I have been investigating is a superconducting solenoid with the following dimensions:

inside diameter	3.2 cm
outside diameter	7.34 cm
length	10.0 cm

With 3×10^5 Ampturns, it is capable of producting a 6 tesla field. The calculated fringing region extends almost 145 cm in front of the lens, though it is essentially negligible until about 50 cm before the lens. For the shape of the axial B-field, see Figure 3.

When the magnet is placed in position in the microprobe, it will sit, inside its dewar, with the leading edge 400 cm from the object slit, and the trailing edge approximately 11 cm

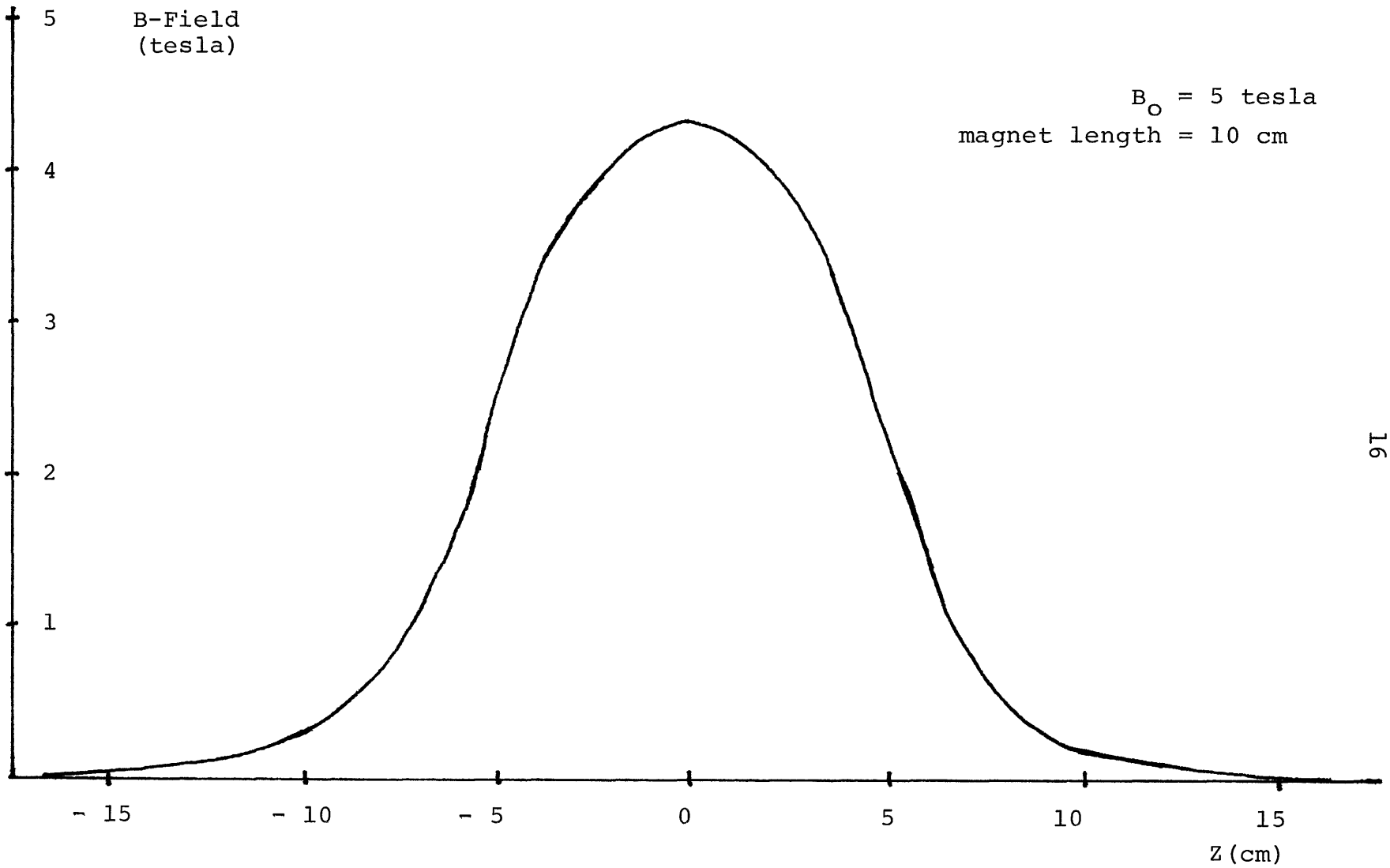

FIGURE 3

AXIAL B-FIELD

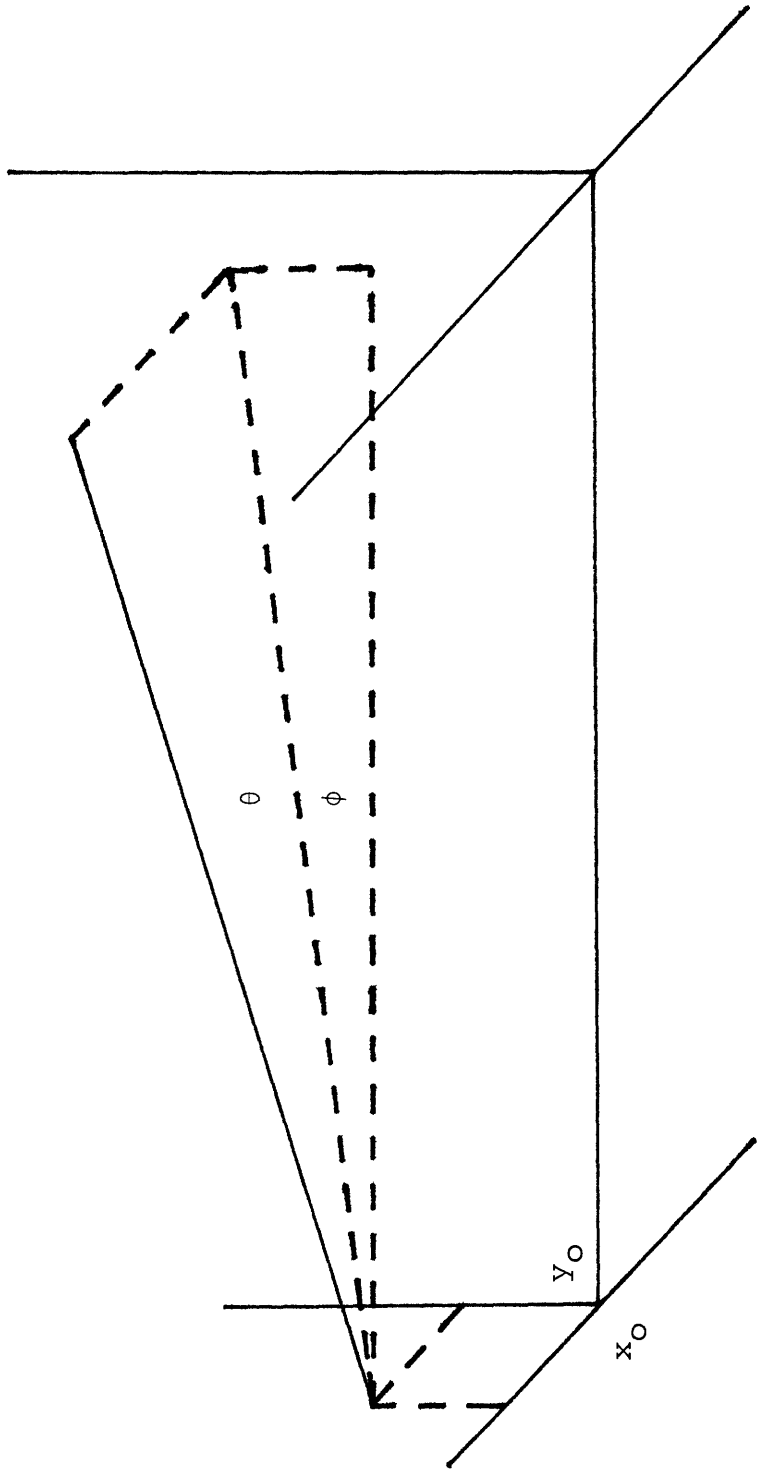

FIGURE 4

THE FOUR COMPONENTS OF A RAY

from the x - y stage upon which the samples are to be placed. (I say approximately because the stage can be moved slightly in the z direction.) A second slit will be placed directly in front of the lens to enable one to change the angle with which the beam strikes the field (the nominal beam divergence is on the order of 2 mr.).

There are no extraneous magnetic fields to interfere with the focusing properties of the lens. Measurement at the site of the microprobe using a gaussmeter with a Hall probe, accurate to .5 gauss, revealed only one significant field in the region of the magnet. However, this field, due to an ion pump on a Kevex Si Li detector, was found to drop off so sharply as to be negligible for distances greater than about 5 cm.

It should be noted here that while the lens has an inside diameter of 3.2 cm, the solenoidal current sheet with the same focusing properties has a diameter given as 5.462 cm. Thus, the RAYTRACE solenoid subroutine is given 5.462 cm as the lens diameter.

DATA

The following parameters were considered in this study: beam position relative to the axis of the solenoid, lens position relative to the beam axis (that is, the tilt of the lens), particle energy, beam dispersion, and, naturally, the B-field. Before these parameters were examined, however, a large number of tests had to be run, in order to insure both that the final data would be meaningful and that it would be as accurate as we might need. The three most important of these are described here.

First, since the RAYTRACE program normally gives an accuracy for x_o and y_o of ± .5 microns, a method for scaling up the entire system was sought. Good results were obtained by multiplying all lengths by some scaling factor, keeping all angles the same, and dividing the B-field by the same scaling factor. The B-field is scaled linearly down because of the following relationship:

$$f \cdot L \propto \frac{1}{B^2}$$

where L is the length of the lens. In interpreting the final figures, specifically x_o, y_o, and the image length, it is necessary to divide by the scaling factor. For simplicity, I have chosen to use a scaling factor of 10.

Second, a test was performed to insure that the output

coordinate system was indeed in the plane of the smallest circle of confusion. Because this coordinate system has its origin at the point where ray 1 (the z axis for most set-ups) and ray 2 cross, it is imperative that ray 2 is chosen correctly. Simple trial-and-error, plus some helpful advice from Professor Harald Enge lead to a choice of .4375 mr for ray 2.

The third test was performed because RAYTRACE integrates ray 2 up to some given integration distance, then traces backwards or forwards using its instantaneous slope at that distance. This integration length (called Z22 in RAYTRACE) then, must be determined if correct results are to be obtained. Again, the trial-and-error method was used to find approximate integration lengths for each configuration.

Before continuing to the discussion of the aforementioned parameters, I must define a term which I will make use of frequently, that being "deviation". So as to represent any particular focus by a single number, I evaluate the following expression, which I call the deviation:

$$D = \sqrt{\frac{1}{N}\sum_{i=1}^{N}(x_{oi}-\bar{x})^2 + \frac{1}{N}\sum_{i=1}^{N}(y_{oi}-\bar{y})^2}$$

where

$$\bar{x} = \frac{1}{N}\sum_{i=1}^{N} x_{oi}$$

$$\bar{y} = \frac{1}{N}\sum_{i=1}^{N} y_{oi}$$

and N is the number of rays. The deviation may be thought of as being similar to an average radius of all rays in the

plane of the output coordinate system. It is a meausre of the "tightness" of the focus of the rays.

The first scan I did examined the relationship between the particle energy, the strength of the B-field (that is, the maximum B-field), and the divergence of the beam. The particle energy was varied through 1 MeV, i.e., approximately ± 5 % of the proton energy. The B-field was varied from 4 to 6 tesla, a reasonable range for our magnet, with $B_{max} = 6$. Finally, both the deviation and the image distance were computed for all combinations of B-field and energy at three values of the divergence, .5 mr, 1 mr, and 2 mr. The data for this scan is found in Tables 1 and 2. The deviations are plotted in Figure 5 (θ = .5 mr), Figure 6 (θ = 1 mr), and Figure 7 (θ = 2 mr). Figure 8 shows the image lengths for the B-field energy combinations. In all four figures, the value to the right of each line is the strength of the B-field in tesla.

TABLE 1

DEVIATIONS FOR ENERGY VS. B-FIELD

ENERGY (MeV)	69.6	69.8	70.0	70.2	70.4	70.6
B-FIELD (tesla)						
	2.33	2.33	2.34	2.34	2.34	2.35
4.0	1.47	1.47	1.47	1.47	1.47	1.47
	3.92	3.92	3.91	3.91	3.91	3.90
	2.11	2.13	2.14	2.14	2.14	2.14
4.5	1.47	1.47	1.47	1.47	1.47	1.46
	4.41	4.10	4.09	4.09	4.08	4.08
	2.10	2.10	2.10	2.08	2.08	2.08
5.0	1.46	1.46	1.46	1.46	1.46	1.46
	4.31	4.31	4.31	4.30	4.30	4.30
	1.88	1.88	1.88	1.87	1.87	1.87
5.5	1.56	1.56	1.56	1.56	1.56	1.56
	4.66	4.66	4.64	4.64	4.64	4.63
	1.83	1.83	1.83	1.83	1.83	1.83
6.0	1.66	1.66	1.65	1.65	1.65	1.64
	5.03	5.03	5.02	5.02	5.02	5.02

NB - For each value of the B-field, the first number is the deviation for a beam divergence of .5 mr, the second for a divergence of 1 mr, the third for a divergence of 2 mr.

TABLE 2

IMAGE LENGTH FOR ENERGY VS. B-FIELD

ENERGY (MeV)	69.6	69.8	70.0	70.2	70.4	70.6
B-Field (tesla)						
4.0	18.59	18.73	18.87	19.8	19.14	19.27
4.5	13.75	13.85	13.95	14.06	14.16	14.27
5.0	10.33	10.41	10.5	10.58	10.67	10.75
5.5	7.82	7.89	7.96	8.03	8.10	8.17
6.0	5.91	5.97	6.02	6.08	6.14	6.20

NB - Image length in cm.

TABLE 3

DEVIATIONS FOR VARYING GUN DISPLACEMENTS

Disp. (cm)	Deviation
.5	40.90
.25	36.66
.05	14.89
.0025	1.68

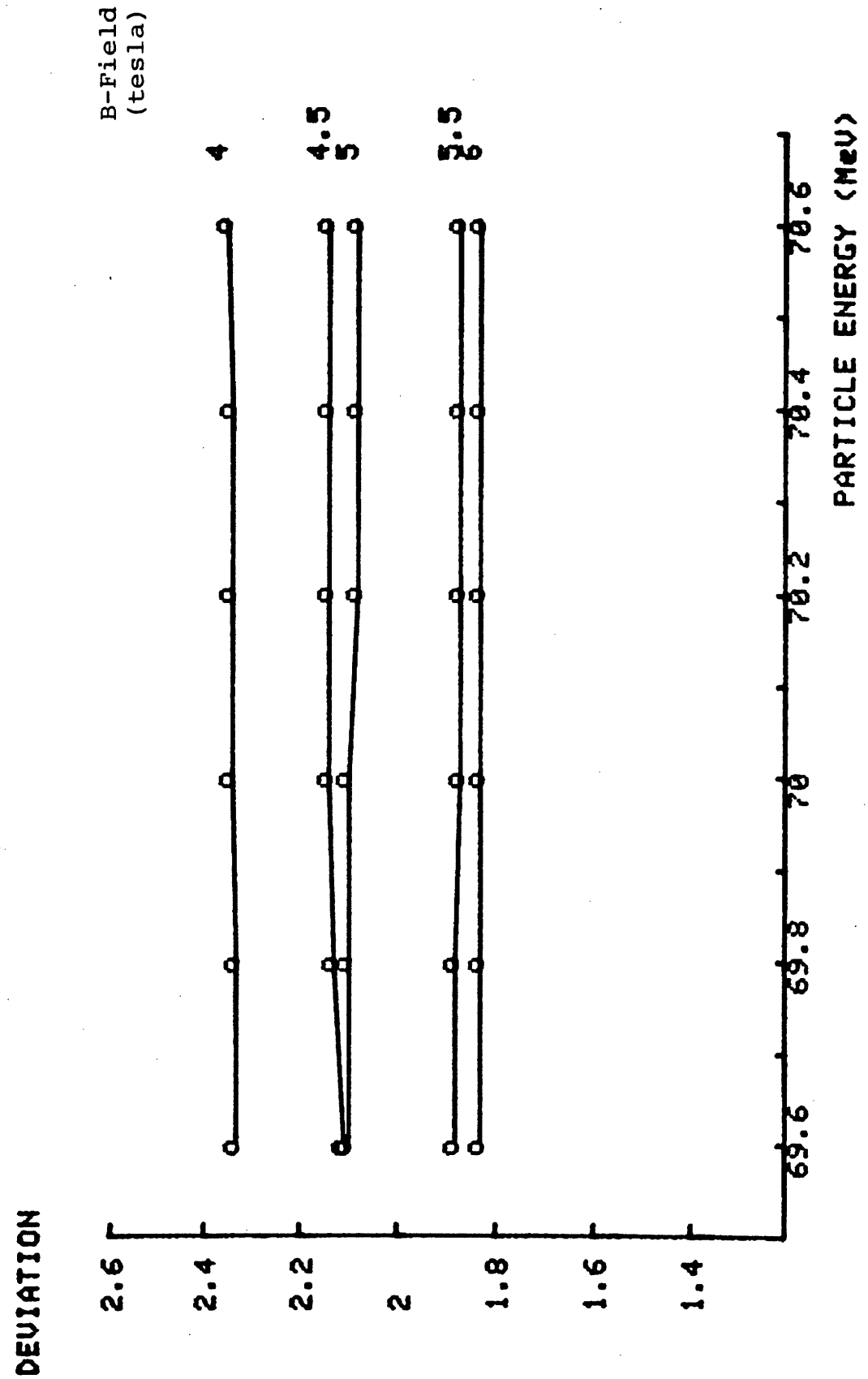
B-Field
(tesla)
4
4.5
5
5.5
6
DEVIATION
2.6
2.4
2.2
2
1.8
1.6
1.4
69.6
69.8
70
70.2
70.4
70.6
PARTICLE ENERGY (MeV)

FIGURE 5

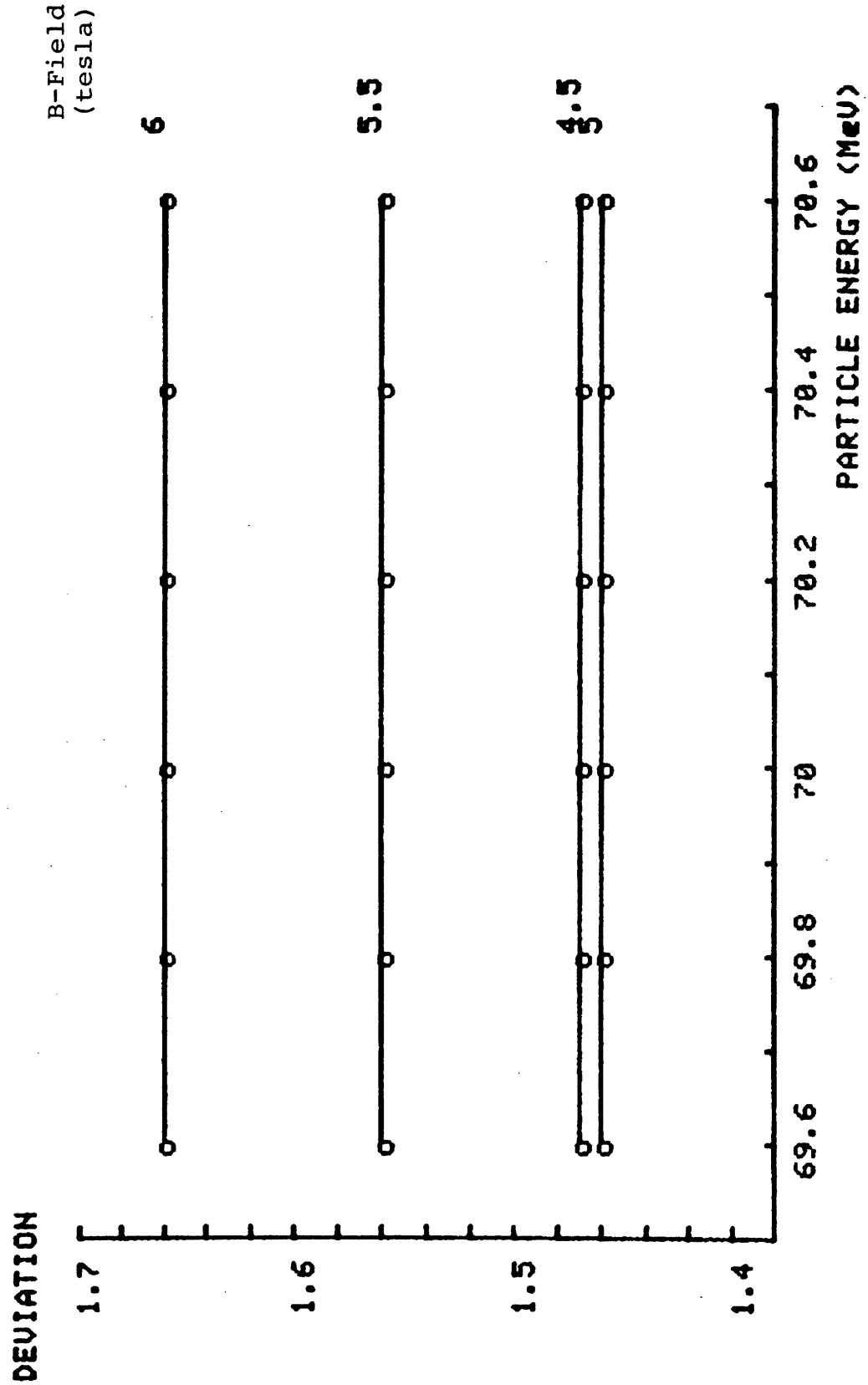
B-Field
(tesla)
6
5.5
4.5
DEVIATION
1.7
1.6
1.5
1.4
69.6
69.8
70
70.2
70.4
70.6
PARTICLE ENERGY (MeV)

FIGURE 6

BLANK PAGE

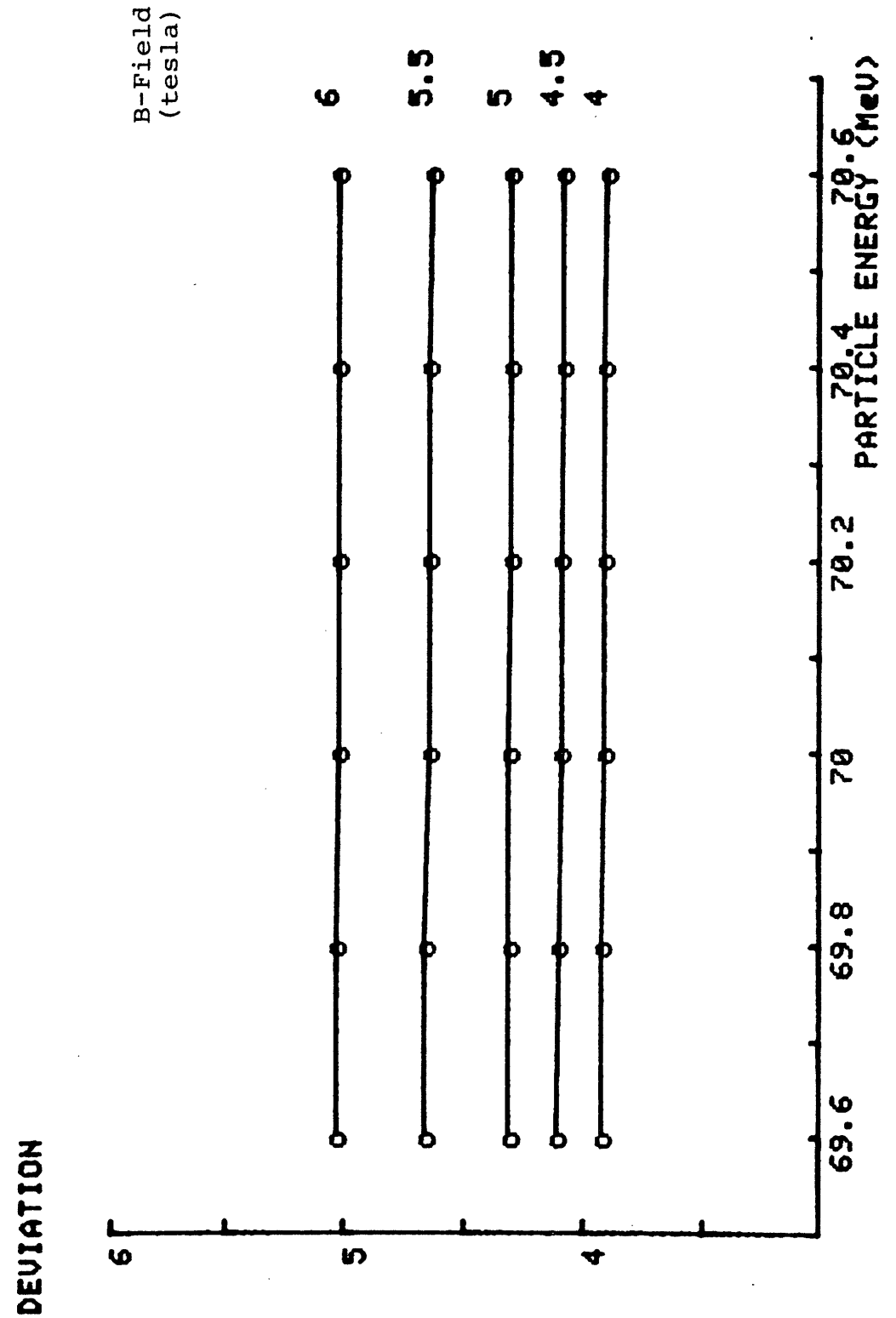
DEVIATION
B-Field
(tesla)
6
5.5
5
4.5
4
6
5
4
69.6
69.8
70
70.2
70.4
70.6
PARTICLE ENERGY (MeV)

FIGURE 7

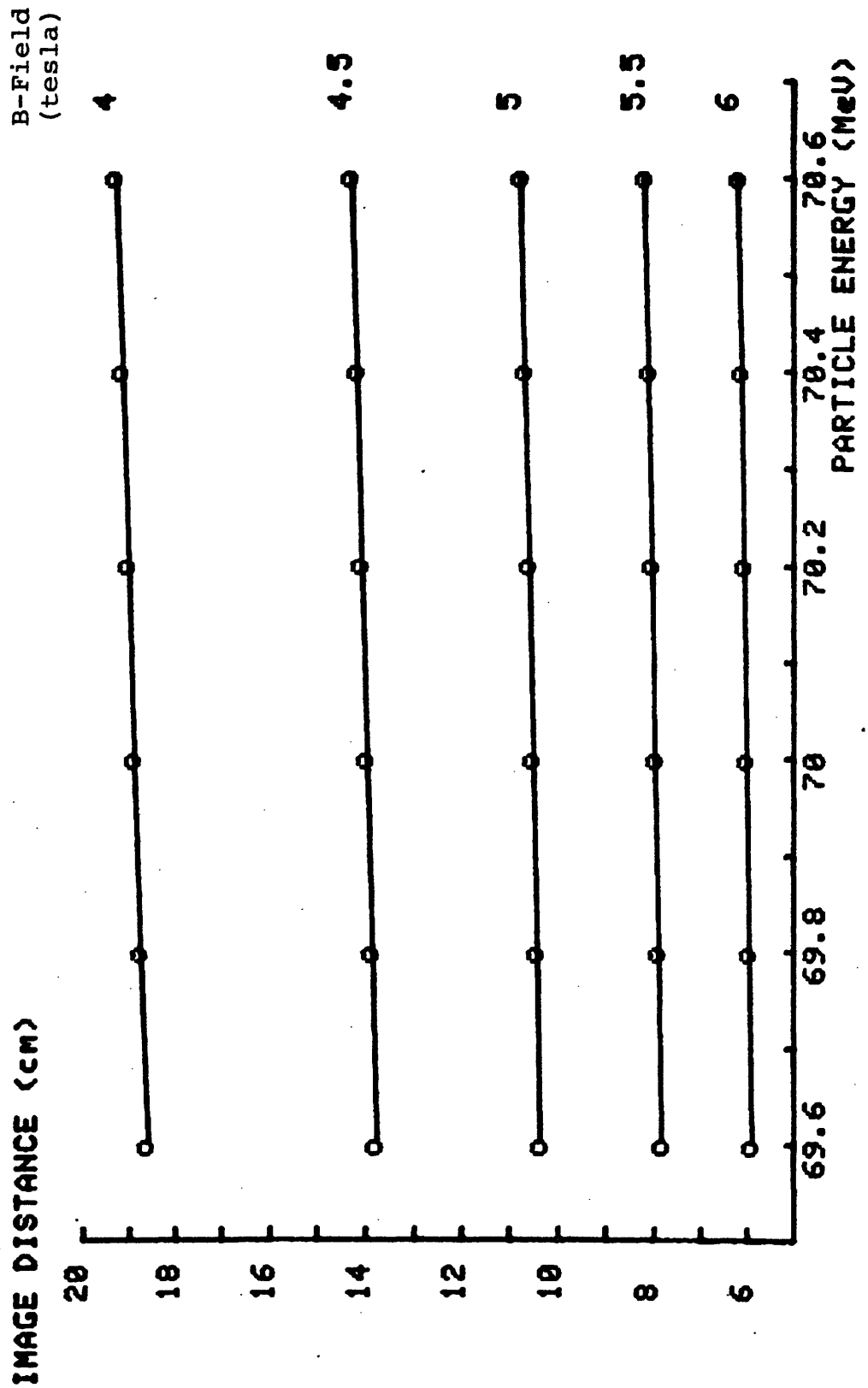
B-Field
(tesla)
4
4.5
5
5.5
6
IMAGE DISTANCE (cm)
20
18
16
14
12
10
8
6
69.6
69.8
70
70.2
70.4
70.6
PARTICLE ENERGY (MeV)

FIGURE 8

By examining these plots, we can deduce the following:

The quality of the focus does not change appreciably as the energy is varied, for constant B-field.

$$\frac{\Delta D}{\Delta E/E} \approx 1.4$$

The best focus occurs with a beam divergence of 1 mr. This is contrary to intuition, as we would expect that the smaller the solid angle of the beam, the smaller the spot size.

The image length closest to the desired value of 11 cm is achieved with a B-field close to 5 tesla.

With these facts in mind, an "ideal" set of these parameters is easily determined.

BF = 4.925 tesla

Energy = 70.0 MeV

Divergence = 1.0 mr

With these values, the deviation is 1.47 and the image length is 10.95 cm. (See Appendix 2 for this run.)

The next scan involved displacing the "gun" which fires the beam by varying distances from the z axis. This would correspond to a shift of the lens perpendicular to the axis, which might arise, for example, from improper alignment of the solenoid. The choice of displacements was made in light of possible errors in alignment. The results, given in Table 3

and shown in Figure 9, while not distressing, are not encouraging either. The deviation, which can be seen to obey

$$D - 147 \propto \sqrt{x}$$

where x is the displacement, becomes large even for relatively small values of x. Thus, the alignment of the lens axis with the beam axis must be done as accurately as possible, as a small error will result in a grossly enlarged image.

The last scan that I performed involved tilting the lens around the y axis by varying angles. The values chosen for the tilt, from .1 mr (corresponding to a shift of one edge of the magnet by .005 mm) to 5 mr (corresponding to a shift of .25 mm) were, again, chosen to be within possible errors due to poor alignment. The deviation as a function of angle of tilt is shown in Figure 10. While these figures also indicate a rapid deterioration of the focus with increasing tilt (even more rapid than with the beam source displacement), they are slightly misleading. The actual final x_o, y_o coordinates of the rays indicate a fairly good focusing of those rays not close to the axis -- the focus is merely displaced from the origin by a distance proportional to the tilt angle. Thus, an error in aligning the magnet in this direction might be compensated for by a shift in the sample.

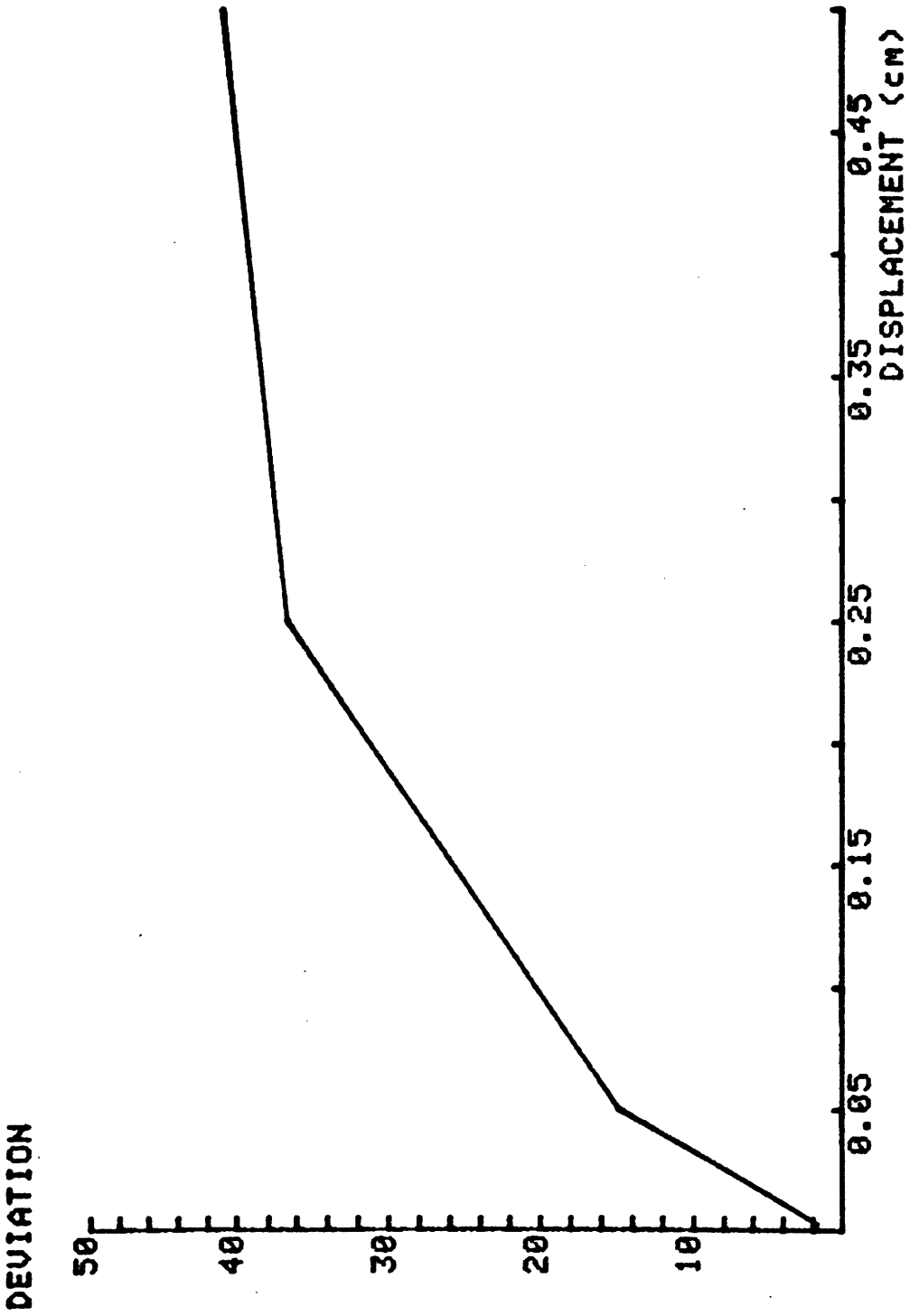

FIGURE 9

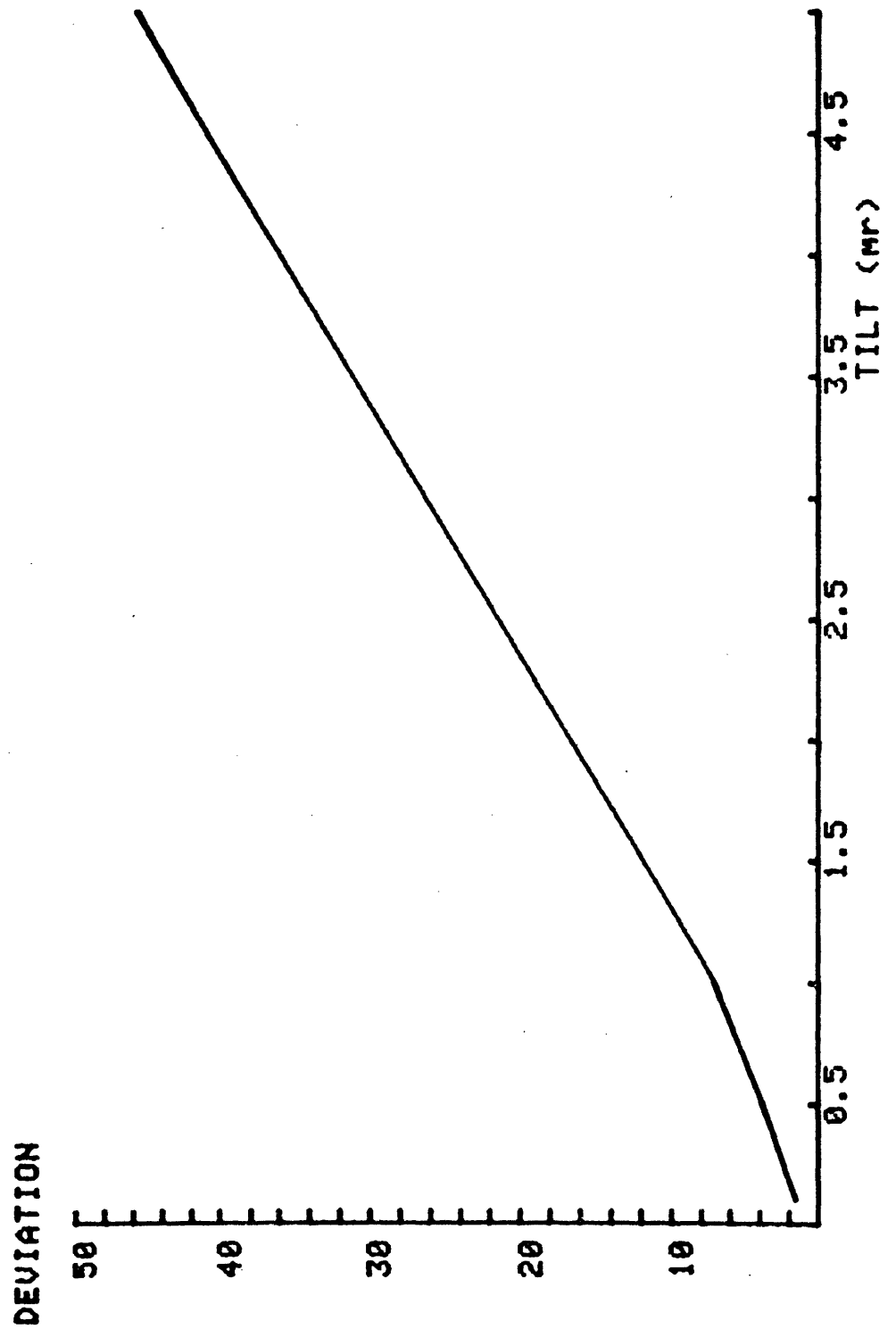

FIGURE 10

CONCLUSION

Given the parameters investigated, an "ideal" focus can be obtained by setting

B-field = 4.925 tesla

Beam Divergence = 1 mr

Particle Energy = 70.0 MeV

In aligning the magnet, great care must be taken, as small errors cause deterioration of spot size.

APPENDIX 1

The derivation given for the trajectory relations, while adequate for the type of geometry I have been studying, does not, in fact, hold true in the general case; that is, where all rays are not forced back to (or close to) the axis. For the sake of completeness, I would like to include the basis for a derivation which takes into account all possibilities. We begin with a statement of the Lorentz force equation

$$m \frac{d\vec{v}}{dt} = q (\vec{v} \times \vec{B})$$

and separate it into component equations in a different way:

$$m (\ddot{r} - \vec{r}\dot{\theta}^2) = q\vec{r}\dot{\theta}\vec{B}$$

$$m(\vec{r}\ddot{\theta} + 2\dot{r}\dot{\theta}) = -q (\dot{r}\vec{B} + \frac{1}{2} \vec{r}\dot{z}\frac{\partial \vec{B}}{\partial z})$$

$$m\ddot{z} = 0$$

Similarities between these and (1a, b, c) are obvious. One may work through these using methods analogous to those I used in the theory section of this paper, to arrive at equations which, in general, include a second-order correction term. For example, the middle equation may be rewritten

$$\frac{\partial}{\partial t} (\vec{r}^2\dot{\theta}) = \frac{-q}{m} (\vec{r}\dot{r}\vec{B} + \frac{1}{2} r^2\dot{z} \frac{\partial \vec{B}}{\partial z})$$

Integrating yields

$$\dot{\theta} = \frac{-q}{2m} \vec{B} + \frac{k}{\vec{r}^2}$$

Using the equality expressed in (8), this becomes

$$\dot{\theta} = \frac{-q}{m} \frac{\vec{A}}{\vec{r}} + \frac{k}{\vec{r}^2}$$

Comparison with (4) shows that k must equal zero when the particle or ray does in fact come back to the axis.

APPENDIX 2

The following is a sample deck and a portion of its resulting output. The parameters are as follows:

B-Field = 4.925 tesla

Solenoid Diameter = 5.462 cm

Integration Length = 11 cm

Particle Energy = 70 MeV

Beam Divergence = 1 mr

```
//TRANS7      JOB (     ,73,10,5000,0100),'KESTEN**',CLASS=A,TIME=10
//          EXEC FORG,LMOD=KARL
//STEPLIB     DD DSN=U.D77917.RAY,DISP=SHR,UNIT=2314                    X
//            VOLUME=SER=RENT2
//SYSIN  DD *
PIXE SOLENOID 50 KILOGAUSS RUN 7                                  SK 11/17/76
   14   500                  1                          MR,MP,NSKIP,JFOCAL,JMTRX
70.0       .1          1.0
SHRT
.0
SHRT
                                                          -63.
SOLENOID
20.0
4000.      110.        100.        54.62       .4925
4000.      110.
SENTINEL
0.
           .4375
           .25
           -.25
           .5
           -.5
                                  .25
            .25                   .25
           -.25                   .25
            .50                   .25
           -.50                   .25
                                  .5
            .25                   .5
           -.25                   .5
/*
```

COORDINATES OPTIC AXIS SYSTEM

	X	THETA	Y	PHI	ZI	DELP	XO	XS	YO	YS	-2 X	2 X	-2 Y	+2 Y
1	0.0	0.0	0.0	0.0	0.0	0.0	0.0	0.0	0.0	0.0	0.0	0.0	0.0	0.0
2	0.0	0.44	0.0	0.0	0.0	0.0	0.0	-10.8056	0.0015	-1.3360	0.022	-0.022	0.004	-0.001
3	0.0	0.25	0.0	0.0	0.0	0.0	0.0001	-5.0393	0.0019	-1.3512	0.012	-0.012	0.005	-0.001
4	0.0	-0.25	0.0	0.0	0.0	0.0	-0.0001	6.0893	-0.0019	1.3512	-0.012	0.012	-0.005	0.001
5	0.0	0.50	0.0	0.0	0.0	0.0	-0.0003	-12.3718	0.0015	-1.3221	0.024	-0.025	0.004	-0.001
6	0.0	-0.50	0.0	0.0	0.0	0.0	0.0003	12.3718	-0.0015	1.3221	-0.024	0.025	-0.004	0.001
7	0.0	0.0	0.0	0.25	0.0	0.0	-0.0019	1.3512	0.0001	-6.0893	-0.005	0.001	0.012	-0.012
8	0.0	0.25	0.0	0.25	0.0	0.0	-0.0010	-5.1509	0.0013	-7.1401	0.009	-0.011	0.016	-0.013
9	0.0	-0.25	0.0	0.25	0.0	0.0	-0.0013	7.1401	-0.0010	-5.1509	-0.016	0.013	0.009	-0.011
10	0.0	0.50	0.0	0.25	0.0	0.0	-0.0013	-11.7922	0.0010	-7.3813	0.022	-0.025	0.016	-0.014
11	0.0	-0.50	0.0	0.25	0.0	0.0	-0.0000	12.9301	-0.0017	-5.0053	-0.026	0.026	0.008	-0.012
12	0.0	0.0	0.0	0.50	0.0	0.0	-0.0015	1.3221	-0.0003	-12.3718	-0.004	0.001	0.024	-0.025
13	0.0	0.25	0.0	0.50	0.0	0.0	-0.0017	-5.0053	0.0000	-12.9301	0.008	-0.012	0.026	-0.025
14	0.0	-0.25	0.0	0.50	0.0	0.0	-0.0010	7.3813	-0.0013	-11.7922	-0.016	0.014	0.022	-0.025

OUTPUT FROM RAYTRACE

REFERENCES

An Introduction to Electron Optics, L. Jacobs, John Wiley and Sons, Inc., New York, 1951.

Electron Optics, P. Grivet, Pergamon Press, New York, 1965.

Classical Electrodynamics, J. Jackson, John Wiley and Sons, Inc., New York, 1975.

Magnetic Spectrographs for Nuclear Reaction Studies, H. Enge, unpublished.

Electron Ray Tracing Through Magnetic Lenses, L. Goddard and O. Klemperer, Proc. Physics. Society, 56, 378 (1944).

Calculation of Fields, Forces, and Mutual Inductances of Current Systems by Elliptic Integrals, M. Garrett, Journal of Applied Physics, 34, 9, p. 2567 (1963).